

Supplementary Information

Hydrogen-bonded Networks of $[\text{Fe}(\text{bpp})_2]^{2+}$ Spin Crossover Complexes and dicarboxylate anions: structural and photomagnetic properties

Verónica Jornet-Mollá, Yan Duan, Carlos Giménez-Saiz, João C. Waerenborgh and Francisco M. Romero*

Table S1 Intermolecular hydrogen bonds in the crystal structure of $1 \cdot 4\text{H}_2\text{O}$.^a

D...A	$d_{\text{D}\cdots\text{A}}/\text{Å}$
N(1)...O(4)#1	2.612(18)
N(5)...O(2)#2	2.768(12)
N(6)...O(3)	2.673(2)
N(10)...O(1W)	2.700(9)
O(1)...O(3W)	2.727(2)
O(2)...O(2W)	2.844(15)
O(2)...O(4W)#3	2.790(2)
O(3)...O(1W)#4	2.745(7)
O(1W)...O(4W)#5	2.717(7)
O(2W)...O(2W)#6	2.861(4)
O(2W)...O(3W)#3	2.842(19)
O(3W)...O(4W)	2.756(13)

^a Symmetry transformations used to generate equivalent atoms:

#1 $x - 1, -y + 1/2, z - 1/2$ #2 $-x, y - 1/2, -z + 3/2$
#3 $x - 1, y, z$ #4 $x + 1, y, z$
#5 $x - 1, -y + 1/2, z + 1/2$ #6 $-x, -y + 1, -z + 2$

Table S2 Intermolecular hydrogen bonds in the crystal structure of $2 \cdot 2\text{MeOH} \cdot \text{H}_2\text{O}$.^a

D...A	$d_{\text{D...A}}/\text{\AA}$
N(1)...O(3)#1	2.649(6)
N(5)...O(4)#2	2.641(6)
N(6)...O(6)	2.679(7)
N(10)...O(8)	2.592(6)
N(11)...O(1)	2.591(6)
N(15)...O(2)#3	2.704(7)
N(16)...O(3S)	2.638(6)
N(20)...O(1W)#4	2.635(6)
O(2)...O(4S)#5	2.731(9)
O(3)...O(1S)#1	2.784(8)
O(5)...O(2S)#3	2.702(6)
O(5)...O(2W)#3	2.811(8)
O(6)...O(1W)	2.793(7)
O(7)...O(3S)	2.591(7)
O(1W)...O(2W)	2.780(8)
O(2W)...O(2S)#6	2.806(8)

^a Symmetry transformations used to generate equivalent atoms:

#1 $-x, -y + 1, -z + 2$	#2 $-x + 1, -y + 1, -z + 2$
#3 $x - 1, y, z$	#4 $x, y + 1, z$
#5 $x + 1, y, z$	#6 $-x + 1, -y, -z + 1$

Table S3 Intermolecular hydrogen bonds in the crystal structure of $2 \cdot 5\text{H}_2\text{O}$.^a

D...A	$d_{\text{D...A}}/\text{\AA}$
N(1)...O(1W)#1	2.651(9)
N(5)...O(2)#2	2.584(11)
N(6)...O(3B)#1	2.885(15)
N(6)...O(9W)#1	2.520(11)
N(10)...O(3A)#3	2.705(13)
N(10)...O(4B)#3	2.567(13)
O(1)...O(2W)	2.938(12)
O(1)...O(3W)	2.924(11)
O(2)...O(1W)#4	2.739(11)
O(3B)...O(8W)#5	2.849(15)
O(4A)...O(10W)	2.572(13)
O(4A)...O(8W)	2.883(15)
O(1W)...O(2W)	2.724(8)
O(3W)...O(3W)#6	2.811(6)
O(4W)...O(6W)	2.702(8)
O(5W)...O(6W)#7	2.960(8)
O(7W)...O(8W)#7	2.910(8)
O(7W)...O(10W)	2.499(8)
O(8W)...O(9W)#1	2.458(7)

^a Symmetry transformations used to generate equivalent atoms:

#1 $x - 1, y, z$ #2 $x, y - 1, z$ #3 $x - 1, y - 1, z$
#4 $x, y + 1, z$ #5 $x + 1, y, z$ #6 $-x, -y + 1, -z - 1$
#7 $-x + 1, -y + 1, -z$

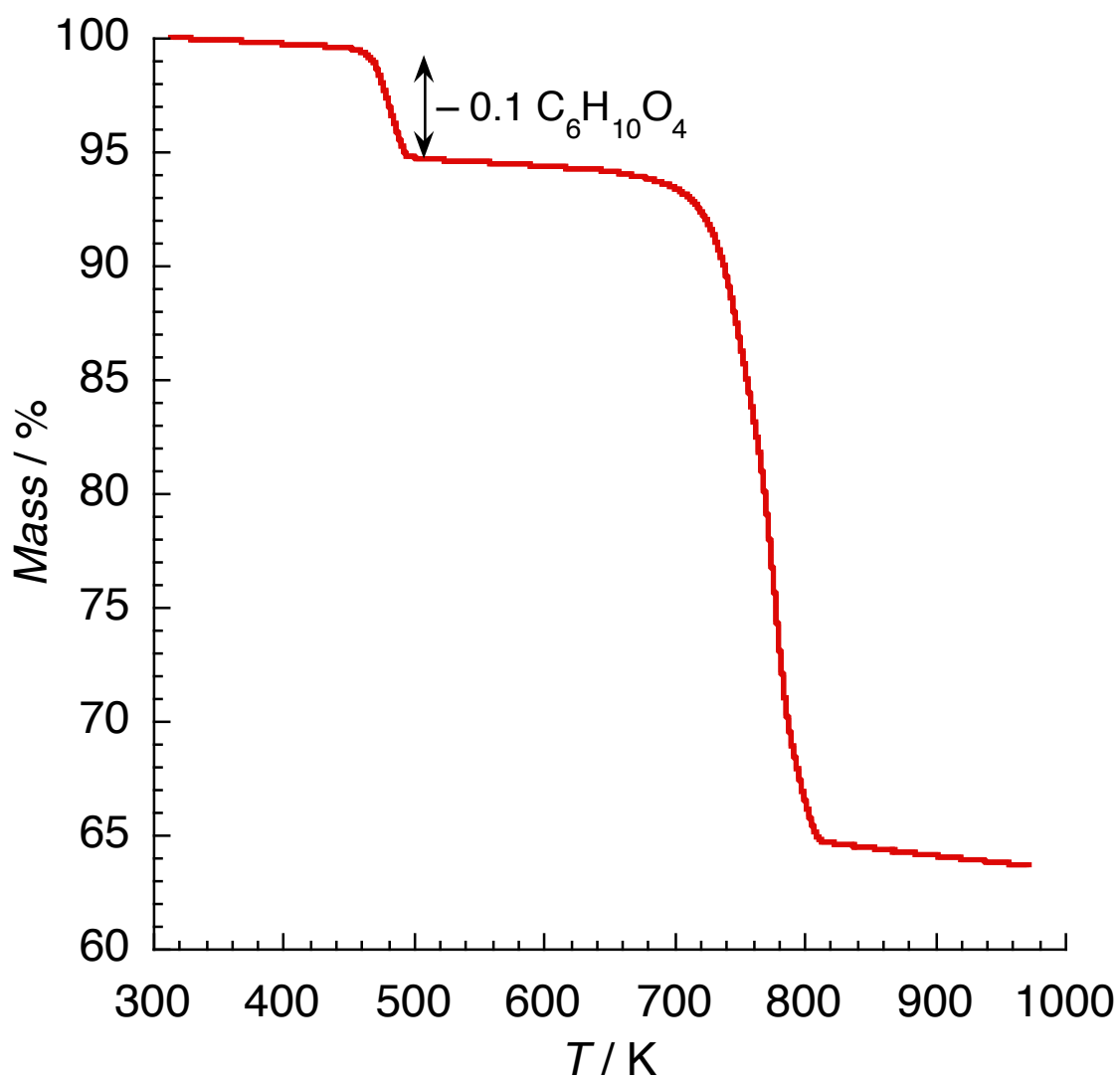


Fig. S1. Thermogravimetric analysis of $\text{Ba}(\text{C}_6\text{H}_8\text{O}_4) \cdot 0.1 \text{ C}_6\text{H}_{10}\text{O}_4$. The plot shows the loss of the adipic acid content. Water molecules of crystallization are not present in this salt.

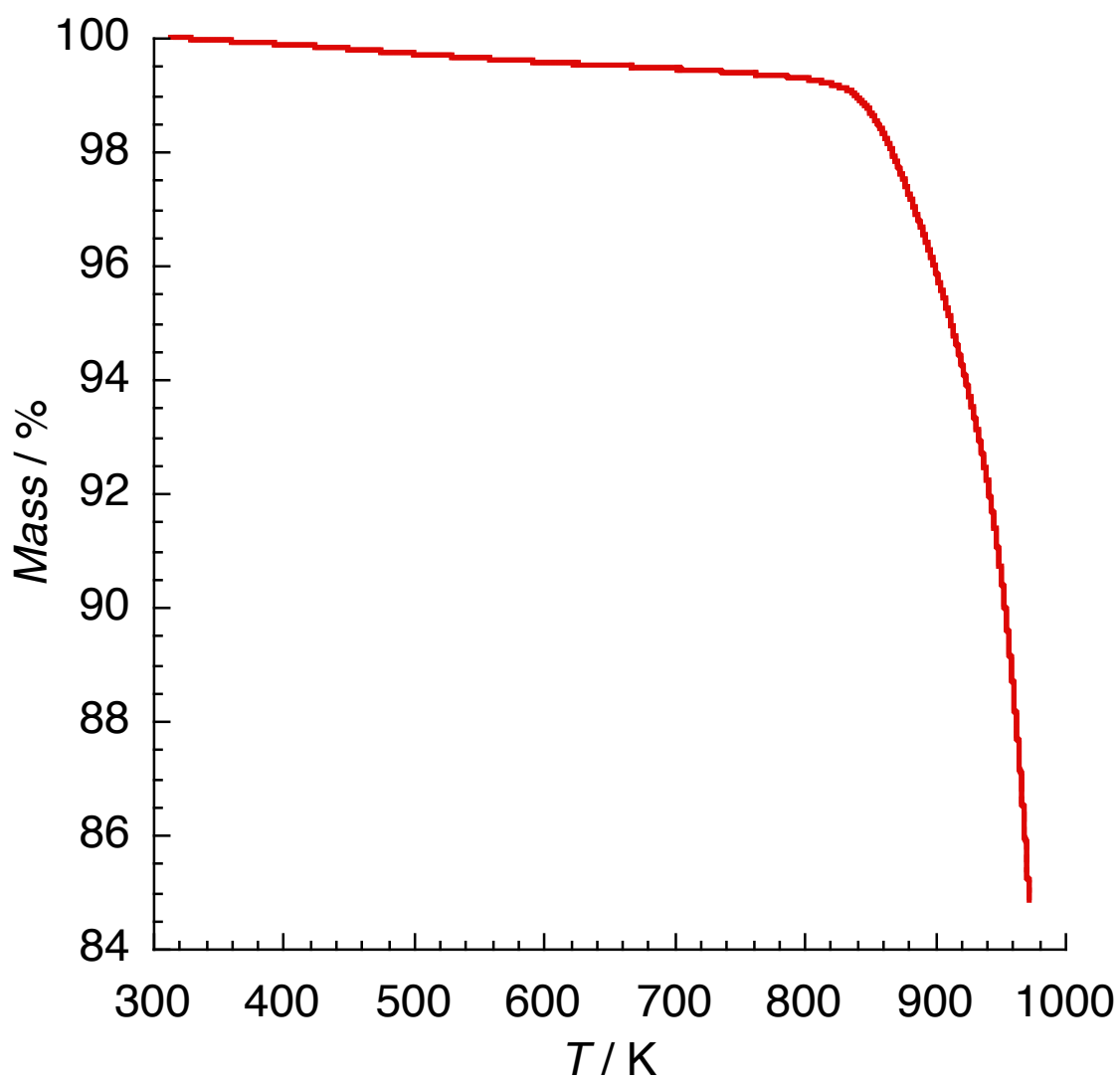


Fig. S2. Thermogravimetric analysis of Ba(C₈H₄O₄). The plot confirms the anhydrous character of this salt.

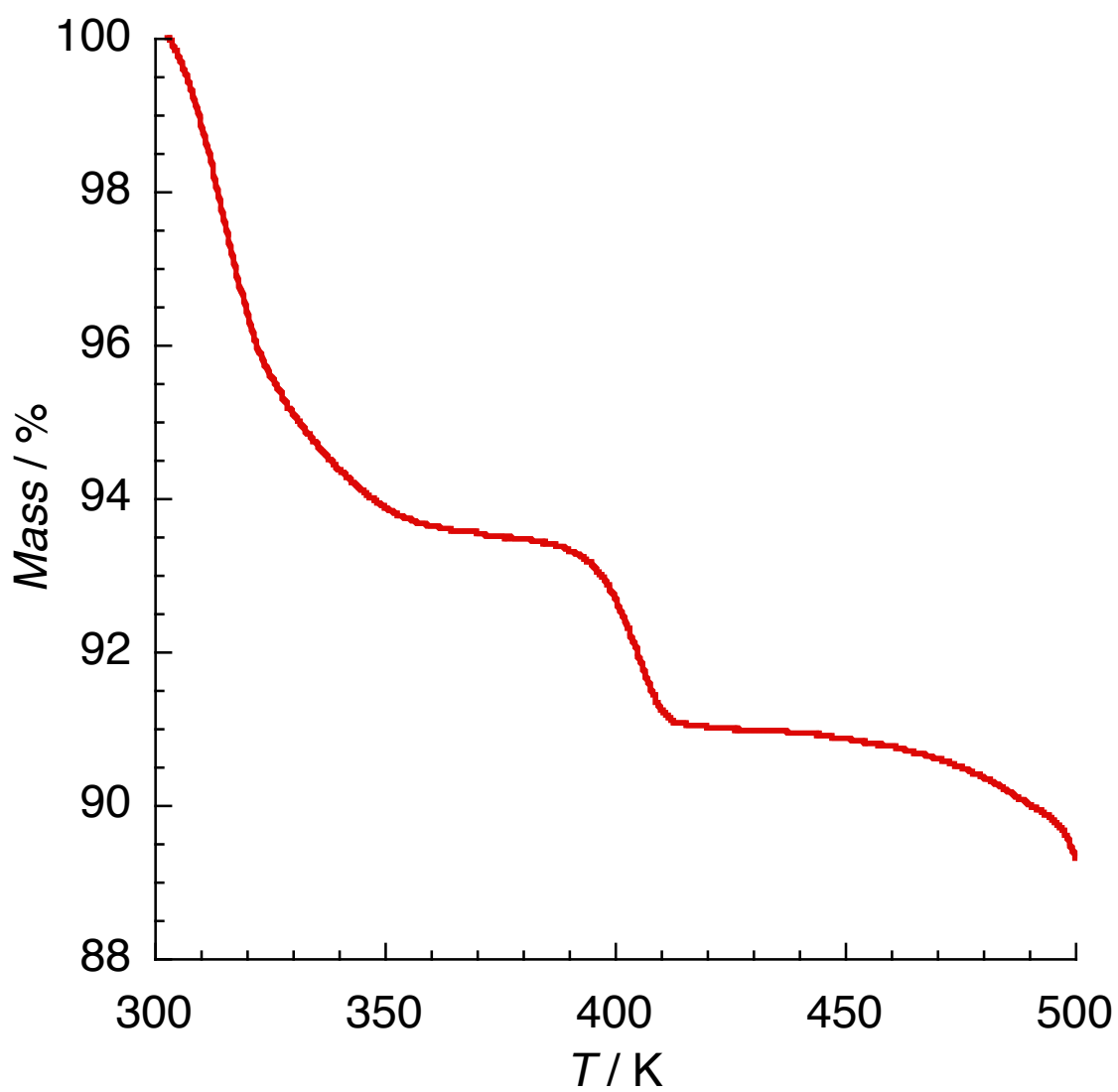


Fig. S3. Thermogravimetric analysis of **1·4H₂O**.

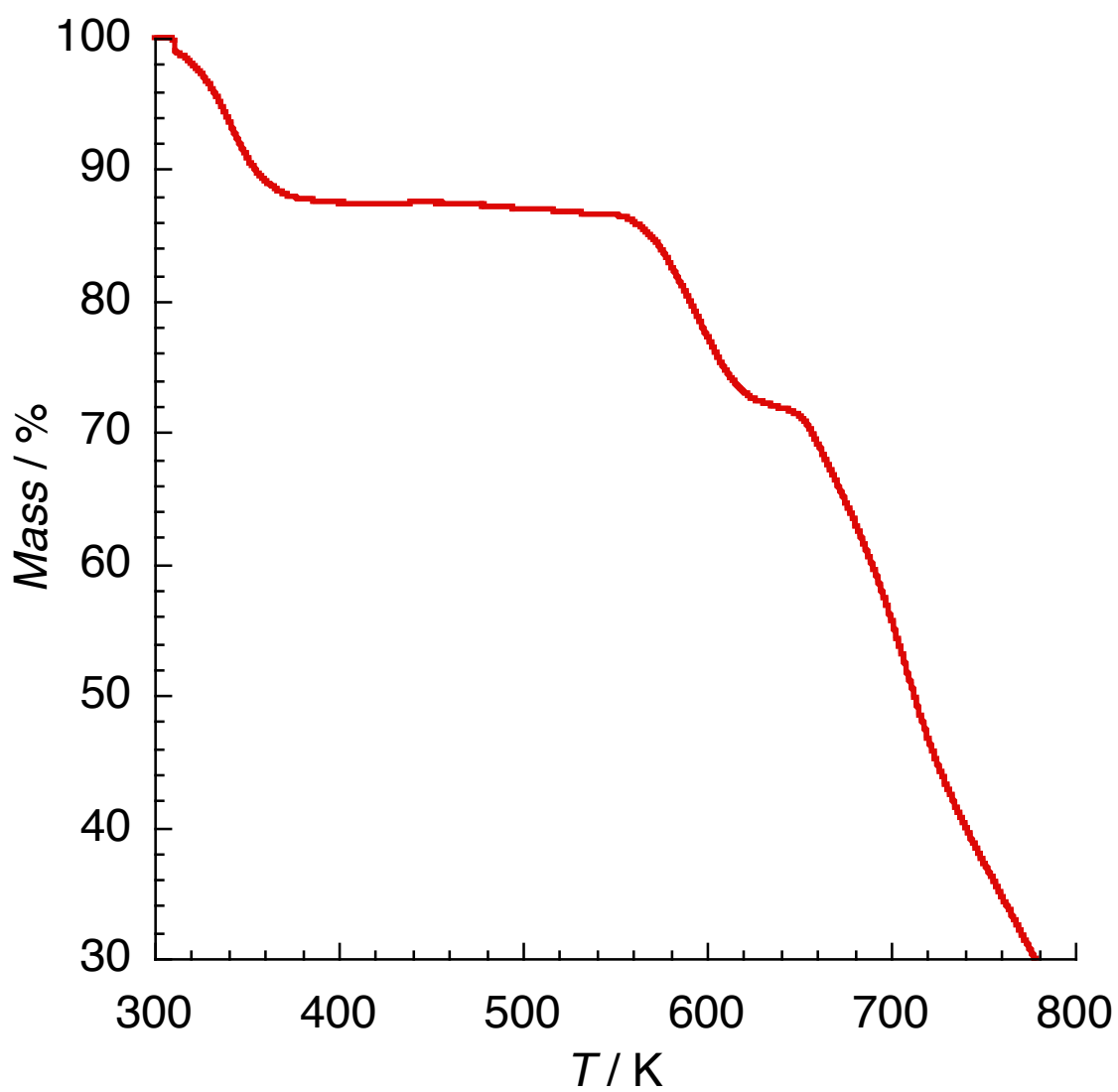


Fig. S4. Thermogravimetric analysis of 2·5H₂O.

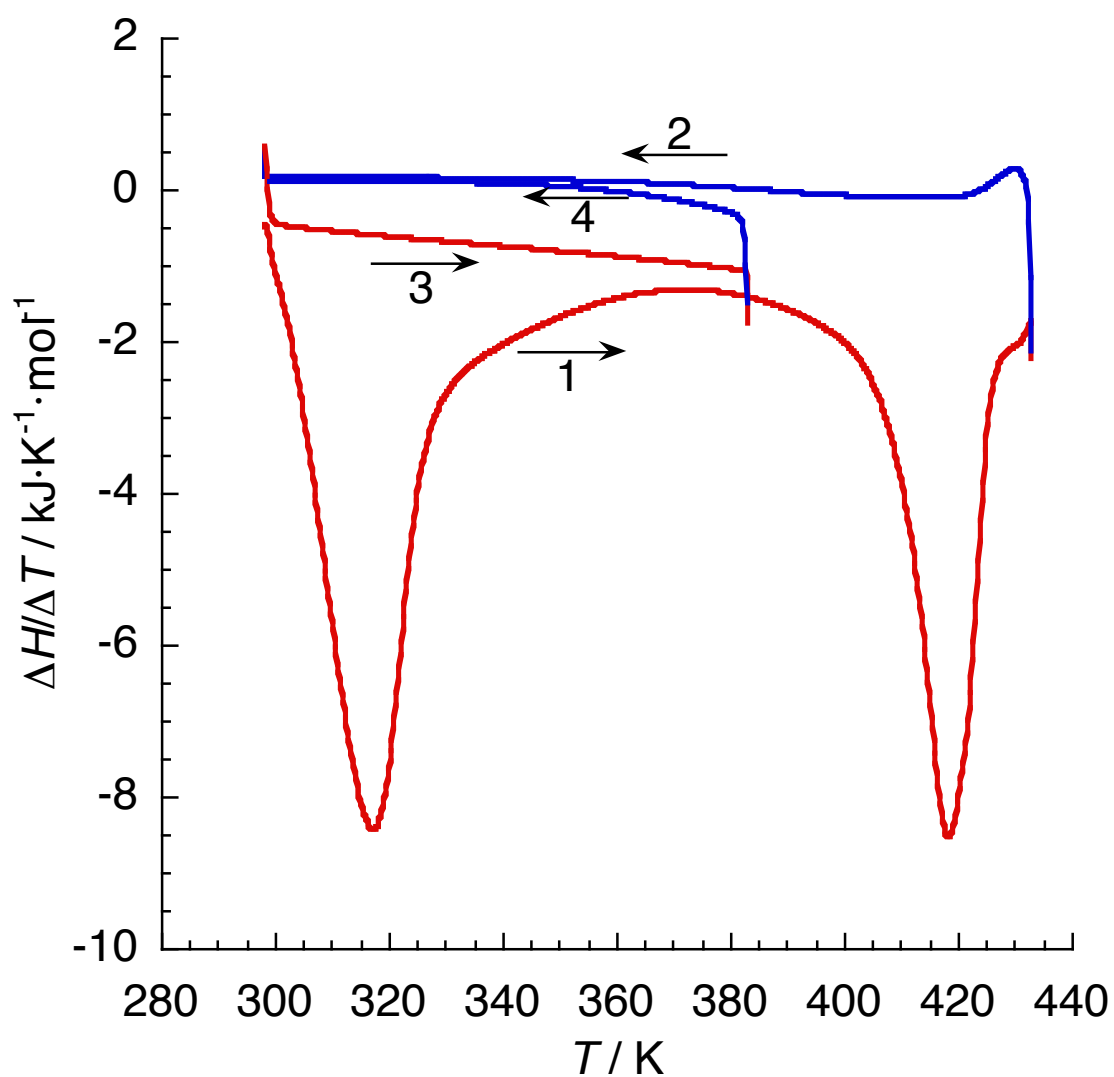


Fig. S5. Differential scanning calorimetry of $1 \cdot 4\text{H}_2\text{O}$. Curve 1: first heating (dehydration process). Curve 2: first cooling. Curves 3 and 4: second temperature cycle.

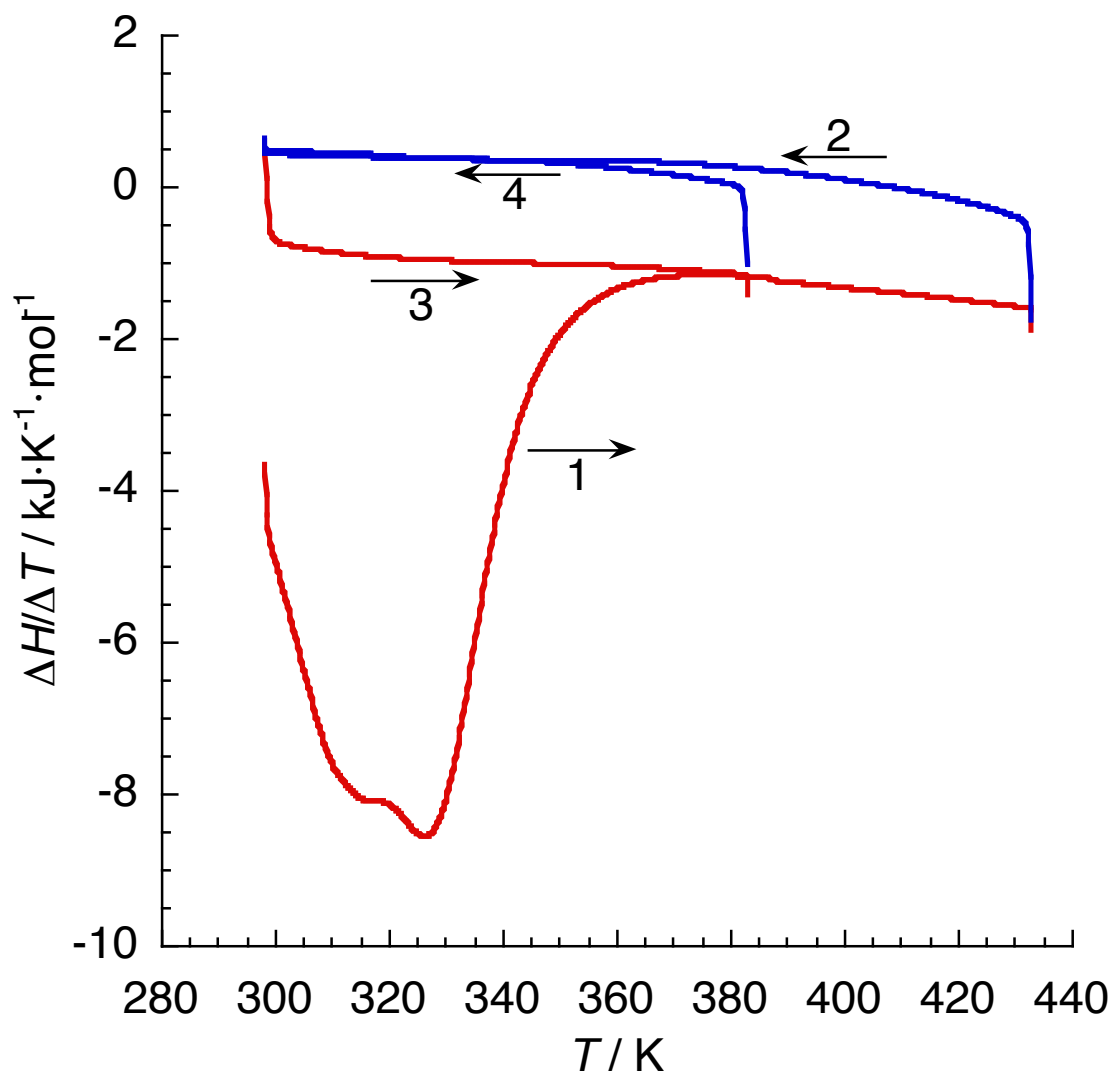


Fig. S6. Differential scanning calorimetry of $2 \cdot 5\text{H}_2\text{O}$. Curve 1: first heating (dehydration process). Curve 2: first cooling. Curves 3 and 4: second temperature cycle.

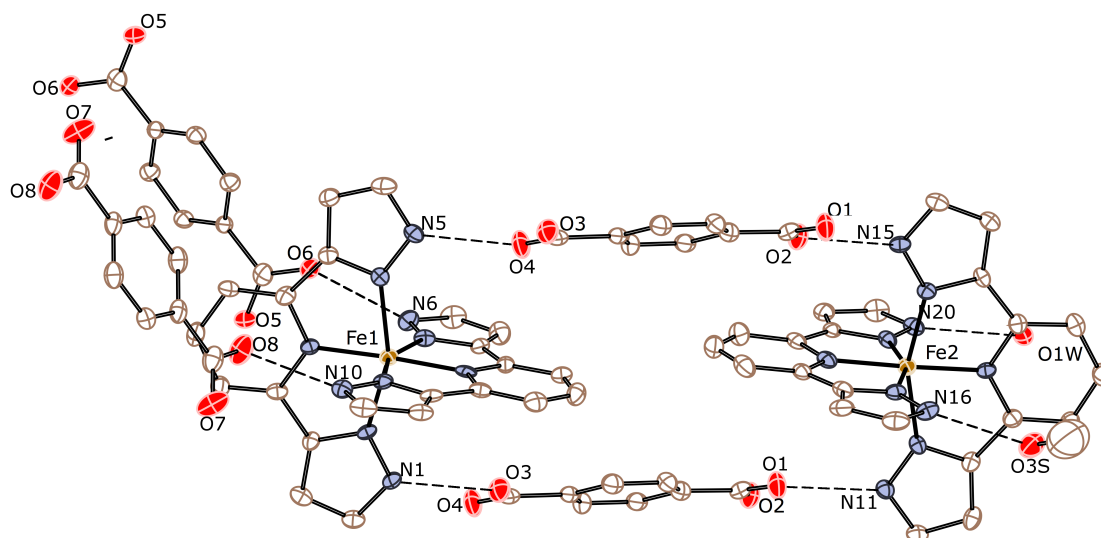


Fig. S7. Thermal ellipsoid plot of the crystal structure of $2 \cdot 2\text{MeOH} \cdot \text{H}_2\text{O}$ showing the two inequivalent $[\text{Fe}(\text{bpp})_2]^{2+}$ cations, the three crystallographically independent terephthalate anions and the two solvent molecules present in the second coordination sphere of the Fe2 site. Dashed lines refer to H bonds. Thermal ellipsoids are drawn at the 50 % probability level.

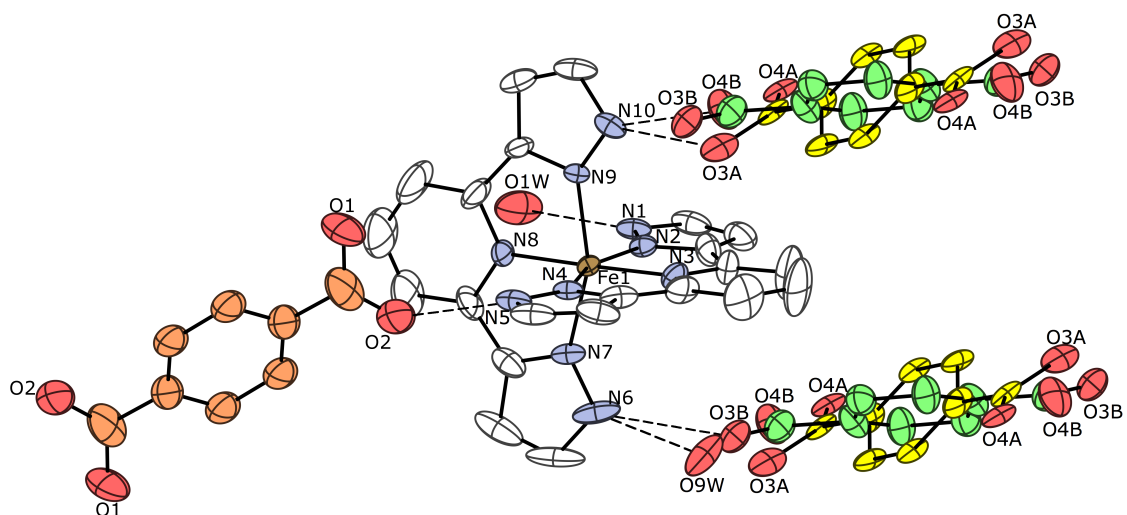


Fig. S8 Thermal ellipsoid plot of the crystal structure of $2 \cdot 5\text{H}_2\text{O}$ showing the second coordination sphere of the iron(II) complexes. Two terephthalate anions are disordered into two positions, A (yellow) and B (green). Thermal ellipsoids are drawn at the 50 % probability level.

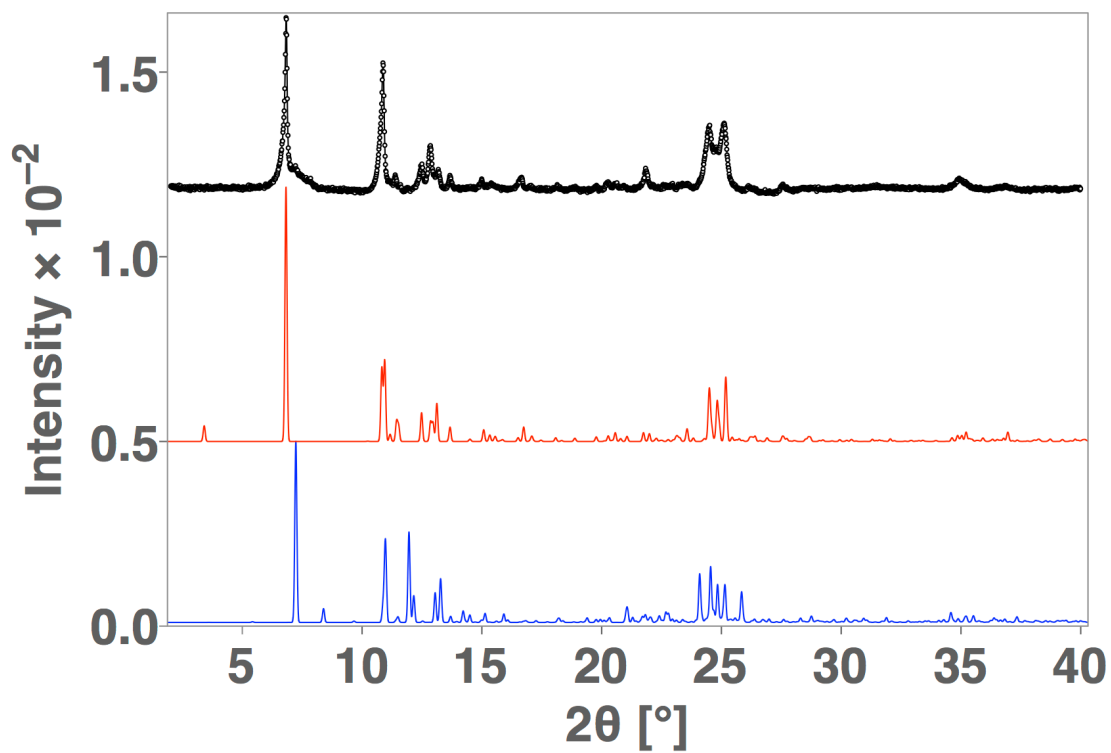


Fig. S9 Comparison of the powder diffractogram of $2 \cdot 5H_2O$ with simulations obtained from single crystal data of $2 \cdot 5H_2O$ and $2 \cdot 2MeOH \cdot H_2O$ (red and blue lines, respectively).

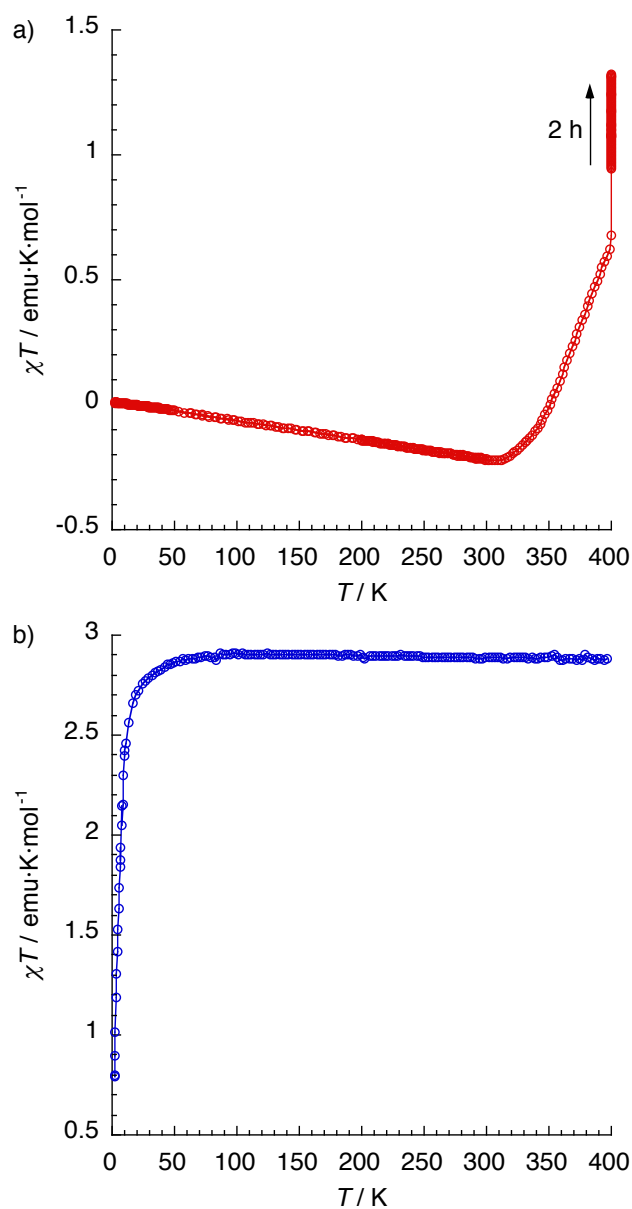


Fig. S10 Thermal variation of the χT product of a) an as synthesized sample of $\mathbf{1}\cdot 4\text{H}_2\text{O}$; b) a dehydrated sample of $\mathbf{1}$. No diamagnetic corrections were applied.

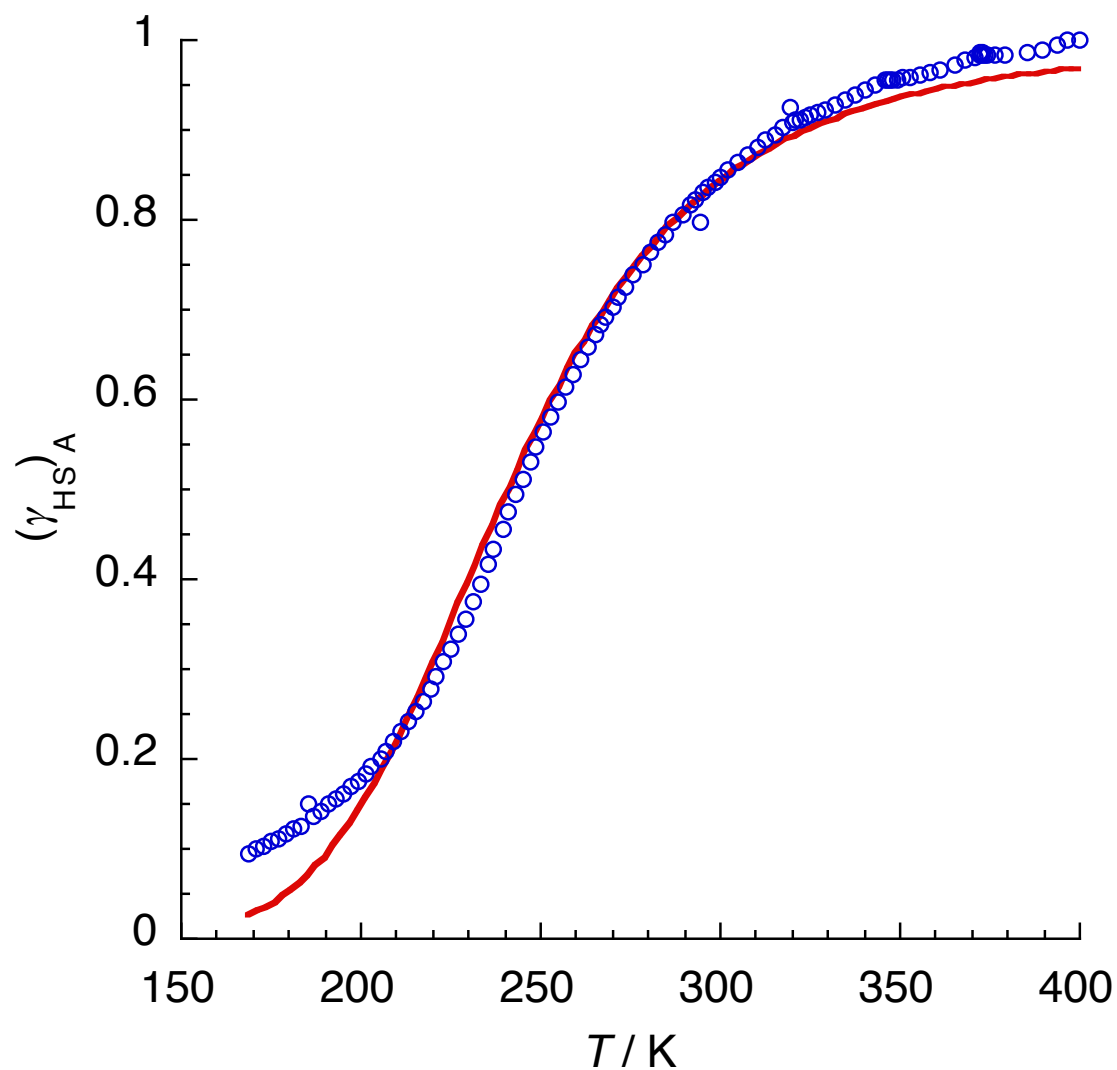


Fig. S11. Temperature dependence of the fraction of high-spin centers corresponding to iron site A, $(\gamma_{HS})_A$, of compound **2**. $(\gamma_{HS})_A$ was calculated from the overall fraction of high-spin centers γ_{HS} following the equation $(\gamma_{HS})_A = 2\gamma_{HS} - 1$. The red line corresponds to the best fit to a Boltzmann distribution with thermodynamic parameters $\Delta H = 17.2 \pm 0.3 \text{ kJ}\cdot\text{mol}^{-1}$ and $\Delta S = 57.8 \pm 1.2 \text{ J}\cdot\text{K}^{-1}\cdot\text{mol}^{-1}$